Article

Numerical Study of Potential Delayed Ettringite Formation in Cemented Nuclear Wasteforms

Abubaker Danfour [1,2,*], Janez Perko [1], Suresh Seetharam [1], Quoc Tri Phung [1], Diederik Jacques [1] and Özlem Cizer [2,*]

1   Belgian Nuclear Research Centre (SCK CEN), Institute for Sustainable Waste Management and Decommissioning (SWD), 2400 Mol, Belgium; janez.perko@sckcen.be (J.P.); suresh.seetharam@sckcen.be (S.S.); quoc.tri.phung@sckcen.be (Q.T.P.); diederik.jacques@sckcen.be (D.J.)
2   Department of Civil Engineering, KU Leuven, 3001 Leuven, Belgium
*   Correspondence: abubaker.danfour@sckcen.be (A.D.); ozlem.cizer@kuleuven.be (Ö.C.)

Abstract: This paper presents a numerical study to investigate delayed ettringite formation (DEF) that may pose a long-term durability risk by altering the microstructure with consequent swelling leading to cracking. A chemo–thermal model is used to predict the evolution and distribution of temperature and hydration phases in a wide range of blended cements. In particular, the influence of nuclear waste loading, waste package size, and the addition of supplementary cementitious materials (SCMs) on DEF is systematically and numerically investigated. The analyses show that higher amounts of ordinary Portland cement (OPC) and waste loadings result in higher hydration temperatures and consequently increased DEF potential by enhancing sulfoaluminate dissolution and hydrogarnet precipitation. Partial replacement of OPC with SCMs reduced hydration heat and mitigated DEF risks. The analysis indicated that the DEF evolution may be different for waste packages of different sizes due to a shift from sulfate-controlling to aluminate-controlling reactions at high temperatures. Interestingly, higher temperatures did not necessarily induce higher DEF potential due to the excessive precipitation of aluminates in the form of hydrogarnet. This research enriches our understanding of DEF's complex behavior, providing valuable insights for engineering applications beyond civil engineering, such as nuclear waste conditioning.

Keywords: delayed ettringite formation; supplementary cementitious materials; cemented waste drums

1. Introduction

Nuclear waste management is considered a major sustainability issue since it is related to the radiological hazards of the waste that can last for long periods, for example, several centuries for short-lived low- and intermediate-level radioactive waste (LLW and ILW) [1,2]. Our research aims to enhance the knowledge of existing waste management practices to improve the basis for the waste acceptance criteria. Nuclear waste immobilization, a key part of radioactive waste management, focuses on creating a durable waste form [3]. Cementitious materials are widely used as immobilization matrices for conditioning low- and intermediate-level radioactive waste because of their availability, high chemical retention of several safety-relevant radionuclides, compatibility with different waste streams, ability to maintain a high pH environment in the disposal facility, and low operational cost [4–7]. However, the cemented waste matrices may reach higher temperatures due to the high heat of hydration, which may result in delayed ettringite formation (DEF), known as heat-induced internal sulfate attack, that may lead to volumetric expansion and hence cracking [8,9].

In Belgium, DEF tests are mandatory as part of waste acceptance criteria to ensure the production of stable nuclear waste drums or packages. This is because DEF can potentially alter the microstructure and transport properties of the waste matrix and may result in undesirable cracks in the cemented wasteform. Although evidence of DEF in such waste

packages is not documented, the consequences have been established in numerous in situ experimental studies on the structural damage due to DEF [9–13].

The degree of DEF depends on various parameters, such as the chemical composition of cement, pore structure, and environmental conditions [14–17]. Early age temperature, whether during cement hydration in mass concrete as a result of cement–waste interaction or during thermal treatment conditions at elevated temperatures, is an important parameter that can promote DEF. The high heat of cement hydration can be encountered in mass concrete with a high cement content where the temperature can exceed 65 °C, which can lead to DEF [18,19]. As it has been shown in previous studies [20–22], partial replacements of supplementary cementitious materials (SCM) such as silica fume, blast furnace slag, limestone, fly ash, and metakaolin can significantly reduce the heat generated during hydration while resulting in equal or even better mechanical properties. In particular, Kolani et al. [23] show the extent of hydration heat reduction with the use of slag-based blended cement. This heat reduction is important for mortars used for the cementation of heavy metal-containing waste to mitigate the potential risks to DEF.

As DEF is a complex phenomenon with multiple contributing parameters, it requires a clear understanding of both individual and synergic contributions among its material and environmental parameters to be able to predict DEF occurrence and evolution. Chen et al. [24] proposed a chemo–mechanical model to quantify the DEF swelling. The model has the capability of detecting damage evolution in concrete attacked by sulfate or other aggressive environments. The damage is derived from the chemical reaction rate. However, the model lacks interaction with temperature, water saturation degree, alkali concentration, and other environmental conditions. Although several thermodynamic models were introduced to better describe different reactions leading to DEF using thermodynamic and kinetic approaches [25,26], they are computationally intensive due to their coupled nature of transport and chemistry. To alleviate the computational issues and consider environmental parameters, a simplified model [27] is implementable in a finite element code to assess DEF in lab-scale concrete samples. Moreover, the model takes cement composition and chemical reaction kinetics into account. So far, the application of the above model is limited to well-controlled laboratory samples.

In Belgium, the cementation of low- and intermediate-level liquid radioactive waste is carried out in 200 L and 400 L drums [4]. In such configurations, the temperature at the core is much higher than at the periphery because of heat loss from the drum walls. Furthermore, additional heat can be generated as a result of the cement–waste interaction. All these factors increase the risk that the heat of hydration exceeds the DEF threshold temperature in cemented waste drums. Therefore, it is essential to couple the thermal and chemical effects on DEF to comprehend the interaction between the hydration heat and DEF practical drum samples on a real scale. Given that we are dealing with Al-rich blended systems, it is worth mentioning that DEF expansion can be suppressed. However, there is a lack of agreement and experimental evidence on the DEF mechanism under suppression effect, according to several studies [28–32]. The absence of consensus regarding the exact suppression mechanism raises a challenge in validating the model using DEF expansion in SCM-blended samples. In the Sellier and Multon model [27], nevertheless, the inclusion of the main DEF species of sulfate and aluminate ions enables the model to reflect the global volumetric fraction of delayed ettringite in SCM-blended systems.

In this study, a benchmarked chemical model was coupled with a hydration heat model to investigate the DEF behavior in real-scale cemented waste drums with different sizes, waste loading, and replacement ratios of SCM. The proposed chemo–thermal model takes into account the temperature during cement hydration and the additional heat generated from the waste and drum scale relevant to waste conditioning, which, to the best of the authors' knowledge, has not been considered in any published work. It is important to acknowledge that the chemical model was developed exclusively for ordinary Portland cement. Nevertheless, the model considers the main species essential for DEF, which ultimately provides a representative and qualitative understanding of DEF behavior within

diverse blended systems. The effects of drum size, waste, and supplementary cementitious materials (SCMs) on temperature and thus on DEF were addressed.

2. Materials and Methods

Figure 1 presents a schematic instruction on the chemo–thermal model and the parameters involved in using primary, binary, and ternary cemented systems with different replacement ratios of SCMs. To study the DEF potential, firstly, the heat evolution and heat rate during hydration of different Portland systems are analyzed. Thermal properties, such as specific heat capacity, heat conduction, and density, that are required to determine heat evolution are estimated using the theory of mixtures, in which the properties of each raw material are multiplied by its volumetric content. The chemical model is based on the content of SO_3, Al_2O_3, Fe_2O_3, and equivalent alkalis of each blended material given in Tables 1 and 2. In this study, the simulated boundary conditions mimic the real conditions of a typical cemented waste drum. The sample is assumed to be fully saturated, and the alkali solid phases are fully dissolved and available in pore solution. Leaching of alkali into the surroundings is neglected since the cemented waste form is sealed inside the steel drum. Although the drum lids are not fully airtight, it is assumed that pre-disposal storage rooms are not compromised.
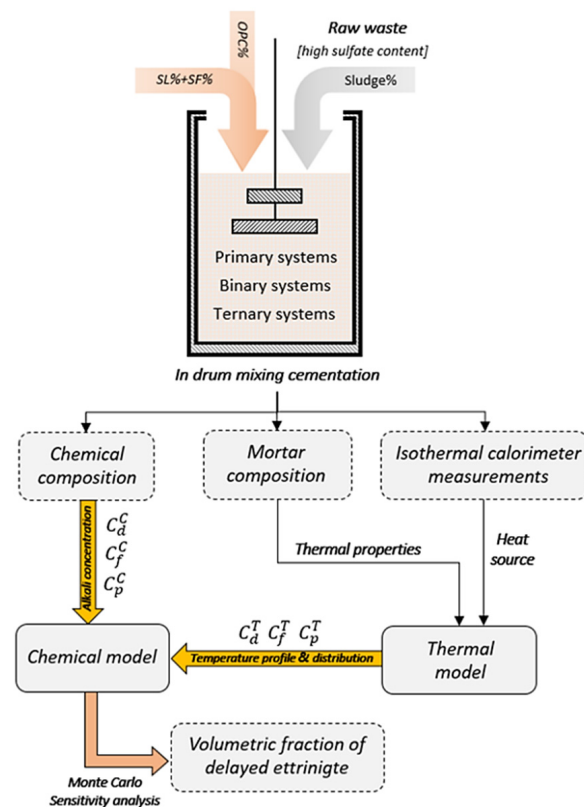
Figure 1. Schematic overview of the chemo–thermal model developed for DEF.

The temperature field of blended cement samples is determined by the thermal model described in [21]. The thermal model is coupled to the equations representing the chemical reactions of aluminate and/or sulfate phases. Temperature evolution, initial alkali concentration, and total sulfate and aluminate contents are used to control the kinetic processes in the chemo–thermal model and the resulting volumetric fraction of delayed ettringite. To study the sensitivity of each of these parameters to the amount of delayed ettringite, a Monte Carlo (MC) sensitivity study is used. MC simulation is an approach that performs multiple model evaluations using random or pseudo-random parameter values from a given probability distribution of model inputs.

Table 1. Chemical composition of OPC, BFS, and SF reproduced from [21].

Chemical Composition	OPC [wt. %]	BFS [wt. %]	SF [wt. %]
CaO	62.91	43.40	0.36
SiO_2	20.59	32.40	96.70
Fe_2O_3	4.98	0.60	0.16
Al_2O_3	3.24	11.10	0.77
SO_3	3.10	2.41	0.24
MgO	1.77	7.77	0.43
K_2O	0.52	0.53	0.91
Na_2O	0.30	0.27	0.20
TiO_2	0.44	1.01	-
P_2O_5	0.30	-	-
Mn_2O_3	0.08	0.32	-
CI	0.07	-	-

Table 2. The chemical composition of nuclear waste sludge reproduced from [22].

Chemical Composition	[mol/L]
Ni	0.40
Cr	0.13
SO_3	0.12
Ce	0.08
Fe	0.05

Sampling for each input parameter is guided by a probability density function (PDF) (i.e., normal, uniform, lognormal, etc.) in which the minimum and maximum values for the parameters are assigned, depending on a priori information from the literature and single simulations. A popular MC class of sampling method named Latin Hypercube Simulation (LHS) was used to create a well-represented input distribution [33,34]. The benefit that arises from using LHS rather than simple random sampling is that estimates formed from the output values of the simulation will mostly have more precision (a smaller variance) with LHS than with simple random sampling. The LHS method assumes that the sampling is performed independently for each parameter and by randomly selecting values from each PDF. An LHS matrix is generated, which consists of a number of rows (N) representing the number of runs and a number of columns (M) corresponding to the number of varied parameters. N model solutions are then simulated using each combination of parameter values (each row of the LHS matrix). The model output of interest is collected for each model simulation.

2.1. Chemical Model

In this work, the chemical model was employed to assess DEF in simulated cemented waste drums. This model computes the chemical evolution of sulfate and aluminate phases in a spatial domain. The model input is the initial amount of primary hydrates (monosulfate, primary ettringite) and ions (free and adsorbed) of aluminate, sulfate, and alkalis in the pore solution. The transport and reaction kinetics depend on temperature, alkali concentration, and relative humidity. Only a brief overview of the model is recalled here; for further details, the reader is referred to [27,35].

As shown in Figure 2, the conceptual model divides the DEF phenomenon into three reaction steps occurring at specific temperature ranges: dissolution of sulfoaluminates (primary ettringite and monosulfate), precipitation of hydrogarnet (precipitation into a low soluble phase), and precipitation of delayed ettringite. The theoretical model uses a set of coupled differential governing equations representing the mass balance for these chemical reactions. The differential equations are based on the stoichiometry of hydration reactions that can be solved iteratively. Sulfates and aluminates are rapidly bound by the

production of these reactions, and their mass transfer can be neglected since their ionic concentrations are about 100 times smaller than the concentration of calcium or alkali. Depending on the total amount of sulfates (S_c) and aluminates (A_c) available in the cement and the conventional alkali concentration (Na_{eq}) in the pore water, the initial amount of the primary hydrates (primary ettringite and monosulfate), secondary hydrates (delayed ettringite and hydrogarnet), and ions is computed using the stoichiometry of the cement hydration reaction in Equations (1)–(3). C, A, S, and H are denoted as CaO, Al_2O_3, SiO_4, and H_2O, respectively.

$$(C_3A)(C\bar{S})_3H_{32} \rightarrow (CaO)_6(Al_2O_3)(SO_3)_3 \cdot 32H_2O, \tag{1}$$

$$C_4A\bar{S}H_{12} \rightarrow (CaO)_4(Al_2O_3)(SO_3) \cdot 12H_2O, \tag{2}$$

$$C_3AS_yH_{4(3-y)} \rightarrow Ca_3(Al_xFe_{1-x})(SiO_4)_y(OH)_{4(3-y)}. \tag{3}$$
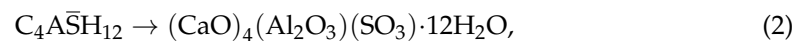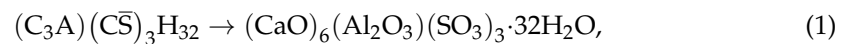
The kinetics of the three stages are controlled by characteristic times, which depend on temperature, alkali concentration from the cement composition, and water content. Each characteristic time in Equations (4)–(6) is defined by three coefficients (C^T, C^H, and C^C) to take the Thermo–Hydro–Chemical (THC) effects into account at each chemical reaction. In total, the model consists of nine activation coefficients, and their determination was derived from previous experiments and theoretical knowledge highlighted by thermodynamic considerations. The coefficients representing the thermal effects on the chemical reactions (C_d^T, C_f^T, and C_p^T) are computed based on Arrhenius law and Van't Hoff law combined as suggested in [27]. As for the chemical effects due to the alkali concentration in the pore solution, their coefficients (C_d^C, C_f^C, and C_p^C) are determined at different temperatures based on experimental analysis. (C_d^C and C_f^C) represents the alkali effect at high temperature during dissolution and hydrogarnet precipitation, respectively. These effects were empirically formulated from the results of [14,15,36]. Moreover, during storage, the alkali effect on the delayed ettringite precipitation rate (C_p^C) was considered in the model as well, based on the experimental results of [16]. As for the influence of water saturation degree, (C_d^H and C_f^H) was assumed to be equal to 1 since the saturation condition does not impact the process of dissolution of ettringite and monosulfate as well as the hydrogarnet precipitation. However, there is a great dependence on saturation during the precipitation of delayed ettrinigte (C_p^H) as found in [37]. The chemical model assumes full saturation conditions due to the high non-linearity of DEF kinetics (C_p^H) concerning the saturation degree. This may pose challenges when predicting DEF in non- or partially saturated conditions, as highlighted in [27].

$$\frac{1}{\tau_d} = \frac{1}{\tau_d^{ref}} C_d^T C_d^H C_d^C, \tag{4}$$

$$\frac{1}{\tau_f} = \frac{1}{\tau_f^{ref}} C_f^T C_f^H C_f^C, \tag{5}$$

$$\frac{1}{\tau_p} = \frac{1}{\tau_p^{ref}} C_p^T C_p^H C_p^C. \tag{6}$$

These activation coefficients allow us to design DEF-accelerated experiments on lab-scale samples and test different types of blended cement and environmental conditions for real scale applications. The reference characteristic times (τ_d^{ref}, τ_f^{ref}, and τ_p^{ref}) are 65 h, 30 d, and 30 h for dissolution of primary hydrates, precipitation of hydrogarnet, and precipitation of delayed ettringite, respectively, as proposed in [27].
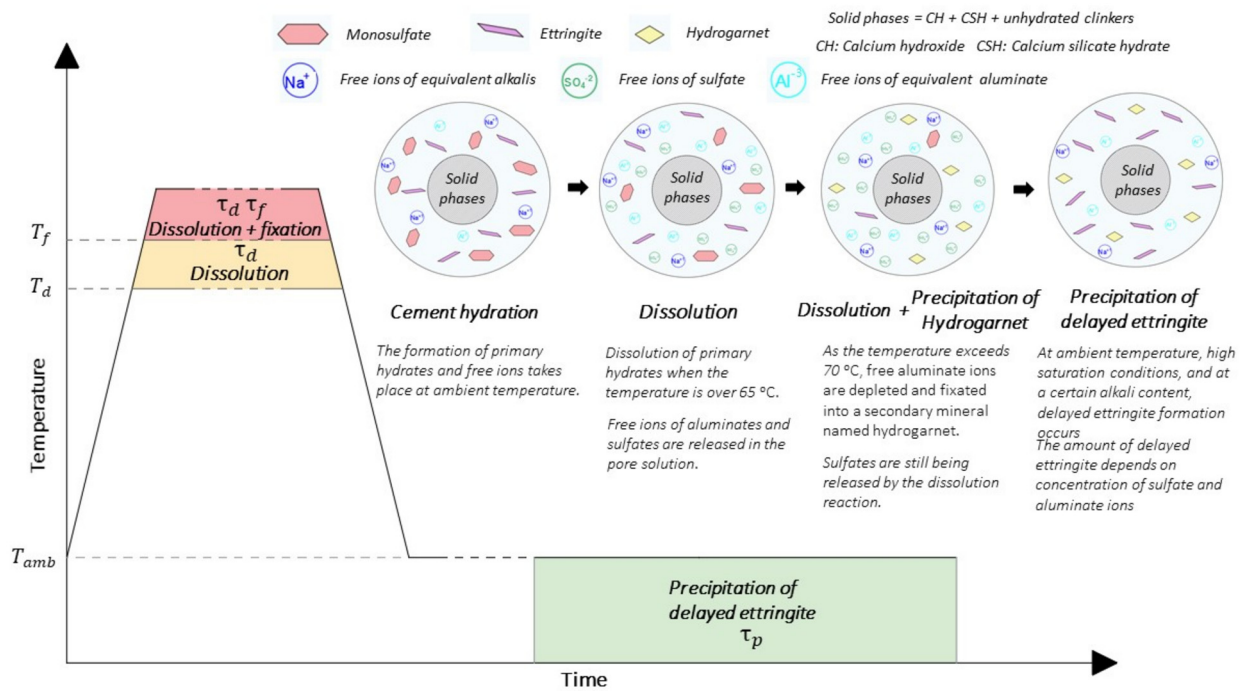
Figure 2. Chemical reactions at different periods in concrete samples subjected to heat treatment lead to DEF.

2.2. Thermal Model with Hydration Heat Source

Temperature evolution in cemented waste drums arising from cement hydration depends on the cement composition, environmental conditions, and any additional heat from the cement–waste interaction. Because DEF depends on the thermal history of the cementitious material, it is important to know the temperature evolution and associated risk of DEF. The evolution of temperature is calculated by the use of a thermal hydration model based on a given cement composition and the addition of SCM.

The evolution of the hydration heat, $Q(t)$ in Figure 3, can be determined through isothermal calorimetry measurements. Phung et al. conducted several isothermal calorimetry experiments on several Portland cement systems (primary, binary, and ternary), including mixtures with waste sludge, to develop an optimum design of recipes for the solidification and stabilization of heavy metal-containing waste sludge [21]. In their work, samples with different water/cement (w/c) ratios (0.7 and 0.9) and replacement ratios of silica fume (SF) (10%, 20%, and 30%) and blast furnace slag (BFS) (30%, 50%, and 70%) were used to assess the effects of SCMs on the rate of hydration heat, cumulative heat release, activation energy, and setting times of blended mortars. Several primary, binary, and ternary cemented systems from this study were chosen, as given in Table 3. The chemical compositions of ordinary Portland cement (OPC), BFS, SF, and waste sludge are presented in Tables 1 and 2. The compositions of cemented waste forms in mass per unit volume are shown in Table 3. High water/cement ratios derive from the high liquid content of the sludge.

Table 3. Compositions of cemented waste forms.

Mix	Waste Loading [Vol.%]	Cement [kg/m^3]	Water [kg/m^3]	BFS [kg/m^3]	SF [kg/m^3]	Fine Agg. [kg/m^3]	Sludge [kg/m^3]
OPC	0	508.5	356.0	0.0	0.0	1351.2	0.0
SF10	0	378.0	378.0	378.0	0.0	42.0	1352.6
SL30	0	286.9	286.9	368.9	123.0	0.0	1394.9
SL30SF10	0	243.0	243.0	364.50	121.50	40.5	1396.6

Table 3. *Cont.*

| Mix	Waste Loading [Vol.%]	Cement [kg/m^3]	Water [kg/m^3]	BFS [kg/m^3]	SF [kg/m^3]	Fine Agg. [kg/m^3]	Sludge [kg/m^3]
SL30SF20	0	200.1	200.1	360.2	121.50	80.0	1398.3
SL50SF20	0	117.3	117.3	351.9	195.5	78.2	1425.6
SL30SF10SLu50	50	446.6	446.6	44.3	223.3	74.4	405.0
SL30SF10SLu45	45	447.9	93.6	223.9	74.6	405.0	467.7
SL30SF20SLu50	50	367.0	37.0	220.2	146.8	405.0	519.8
SL50SF20SLu50	50	289.5	30.0	361.9	72.4	405.0	519.8
SL50SF20SLu45	45	214.8	72.3	358.0	143.2	405.0	467.7
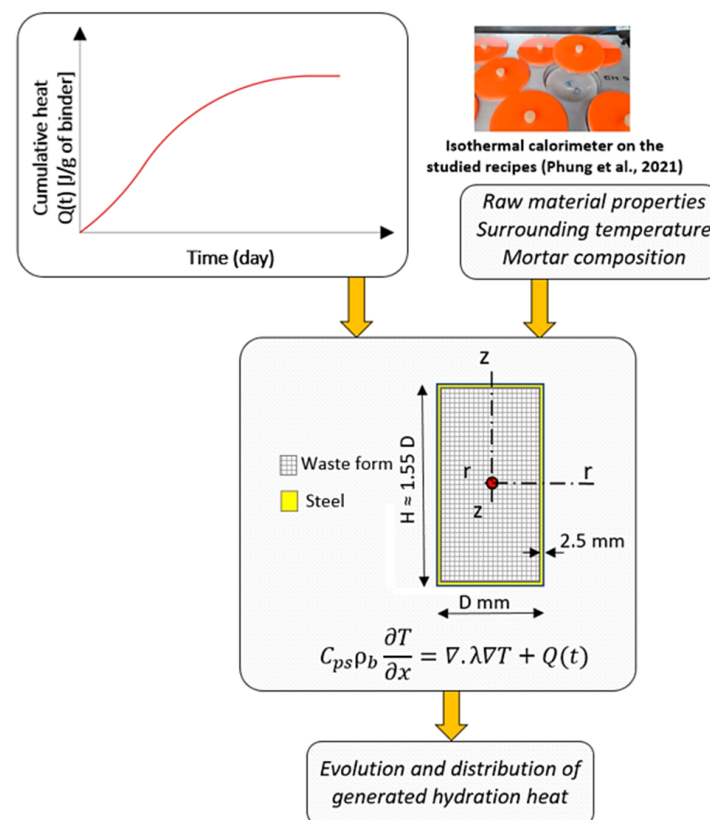
Figure 3. Schematic procedure of the hydration heat model [21].

The cumulative heat release function can be determined by a three parameter equation similar to the one used by Hansen and Pedersen for describing the strength development in concrete (Equation (7)). The equation is used to describe the development of the hydration degree (α), as proposed by Phung et al. [17]. The total heat ($Q(t)$) evolution represents the heat source of the thermal model that is attributed to the heat contributions from all different exothermic reactions of binders (OPC, BFS, SF, and sludge).

$$Q(t) = Q_u e^{-\left[\frac{\tau}{t_{eq}}\right]^{\beta}}. \tag{7}$$

Q_u is the ultimate hydration heat [J/g] that the cemented waste can release during hydration and $\dot{\alpha}$ is the rate of overall hydration degree. t_{eq} is the chronological time or so-called equivalent age [h], τ is the characteristic time parameter [h] for a given isothermal temperature, T_c, at which a calorimeter experiment is carried out, and β is an empirical parameter. Table 4 consists of all the input parameters used in the thermal model. The equivalent age, t_{eq}, can be computed using the maturity index function, which is temperature-dependent and based on the Arrhenius Equation (8). This equation is a com-

mon approach to considering the temperature sensitivity of the combined rate of hydration due to all exothermic chemical reactions.

$$t_{eq} = e^{\frac{E_a}{R}\left[\frac{1}{T_c} - \frac{1}{T}\right]} \Delta t. \tag{8}$$

To define the temperature sensitivity of the reaction, an activation energy, E_a, is determined via Equation (9). The method was developed based on a modification of ASTM C 1074 using isothermal calorimetry data [38].

$$E_a = -\frac{ln(\tau)}{(1/T_c)}. \tag{9}$$

Finally, the temperature field in the waste drum is predicted from the heat balance equation in Equation (10).

$$\rho c_{ps} \frac{\partial T(x,t)}{\partial t} = -\nabla \cdot \vec{q}(x) + \dot{Q}(t), \tag{10}$$

$$\dot{Q}(t) = \frac{\partial \alpha(t)}{\partial t} w_b Q_u. \tag{11}$$

w_b is the total amount of binder in the sample. The binder represents OPC and SCM combinations. Using Fourier's law for an isotropic material

$$\vec{q}(x,t) = -\lambda(x)\nabla T(x,t). \tag{12}$$

Table 4. Model parameters used in the thermal model.

Parameter	Description	Unit	Range	Equation
E_a	Activation energy	kJ/mol	40–50	(9)
R	Ideal gas constant	J/mol·K	8.314	(8)
T_c	Reference temperature	°C	20	(7) and (9)
τ	Time parameter	hour	0.72–2.50	(9)
β	Empirical shape parameter	-	0.30–1.15	(7)
Q_u	Ultimate hydration heat	J/g	320–690	(7) and (11)
w_b	Binder weight	kg/m³	0.7, 0.9	(11)
C_{ps}	Effective heat capacity	J/kg·K	860–1170	(10)
λ	Effective thermal conductivity	W/m·K	1970–2215	(12)
α	Hydration degree	-	0.0–1.0	(10)

3. Results and Discussion

In this section, several effects on the heat generated during cement hydration and, thus, on DEF are addressed in detail. In the chemo–thermal model, the surroundings and initial temperature are considered ambient. Moreover, other initial conditions that represent the initial amount of primary and secondary hydrates, as well as free ions, are stoichiometrically determined depending on the sulfate and aluminate molar ratio (S_c/A_c) that is provided in Table 5. In addition, the leaching of alkali is neglected for cemented waste mixes since the simulated samples are considered to be sealed inside a drum and not exposed to the outside environment. Finally, all blended samples used in this study are assumed to be fully saturated.

**Table 5.** The concentration of chemical compounds in different cement mixtures.

| Mix	SO_3 [%]	Al_2O_3 [%]	Fe_2O_3 [%]	Na_{eq} [mol/L]	Ø [%]	S_c [mol/m³]	A_c [mol/m³]	$\frac{S_c}{A_c}$
OPC	3.10	3.24	4.98	0.35	25.0	165	267	0.62
SL30	2.89	5.60	3.67	0.34	24.0	148	319	0.47
SF10	2.81	2.99	4.50	0.35	25.0	147	242	0.61
SL30SF10	2.61	5.35	3.18	0.35	24.0	132	293	0.45
SL30SF20	2.32	5.11	2.70	0.35	24.0	116	368	0.43
SL50SF20	2.18	6.68	1.83	0.35	23.0	106	300	0.35
SL30SF10SLu50	1.54	3.15	1.87	0.54	28.0	250	538	0.46
SL30SF10SLu45	1.60	3.29	1.96	0.54	28.0	250	540	0.46
SL30SF20SLu50	1.36	2.99	1.58	0.55	28.0	220	490	0.45
SL50SF20SLu50	1.44	4.03	1.34	0.54	28.0	231	595	0.39
SL50SF20SLu45	2.18	6.68	1.83	0.54	28.0	202	550	0.37
OPC—concrete [1]	3.46	4.3	3.80	0.91	14.6	177	270	0.66
OPC—concrete [2]	3.36	4.1	3.75	0.69	14.0	168	255	0.66
OPC—concrete [3]	3.46	4.3	3.80	0.84	15.2	177	270	0.66

[1]: [36] [2]: [14] [3]: [15].

3.1. Hydration Heat Evolution

Figure 4a presents the temperature evolution of OPC samples with different cement weights per cubic meter in concrete mix compositions. The predicted temperature profiles shown in Figure 4a are taken at the core (0.0, 0.0) shown in Figure 3 of the sample, where the temperature is expected to be the highest. In the figure, it can be predicted that the maximum temperature during hydration increases with the amount of cement in the system. This implies that in OPC samples with a low volume fraction of aggregates and, hence, a larger volume fraction of cement, the hydration heat is high. In addition, since the thermal model assumes complete hydration ($\alpha(t_n) = 1.00$) of cement particles, the heat rate is proportional to the cement content as well, as shown in Figure 4b.

The effect of SCM (SF, BFS, and combined) replacement levels on the evolution of temperature is presented in Figure 5a. It can be seen from the figures that the maximum early temperature during hydration is reduced in binary and ternary systems, which implies that BFS and SF play a crucial role in reducing the hydration heat. The results show that incorporating 10% SF (SF10) and 30% BFS (SL30) decreased the maximum temperature by ~13 °C and 20 °C, respectively. The maximum temperature tends to decrease further in ternary blended systems. Figure 5b also shows a reduction in the heat rate, which indicates changes in the chemical reactions in binary and ternary blended systems. This is in agreement with previous studies that reported a temperature and heat rate decrease with the addition of SF to OPC systems [20,21,39].
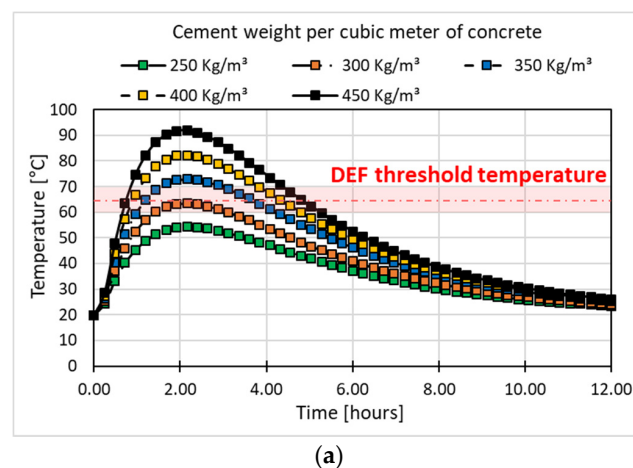
(a)

Figure 4. *Cont.*
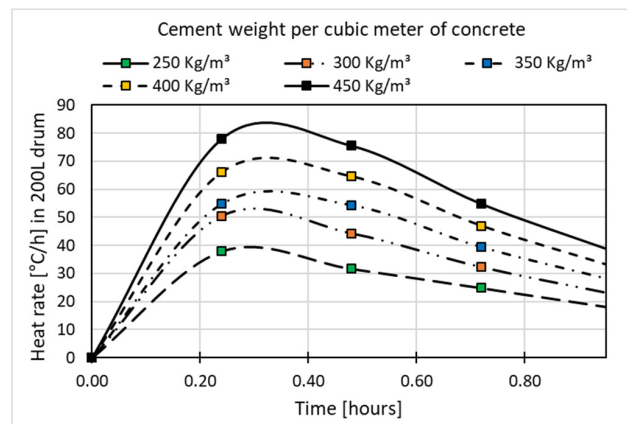
(**b**)

Figure 4. (**a**) Temperature evolution in OPC samples with different cement content. (**b**) Heat rate at early hydration of OPC samples with different cement content.
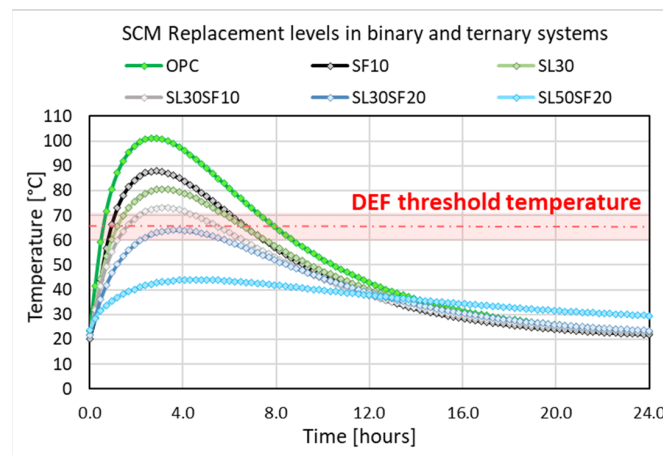
(**a**)
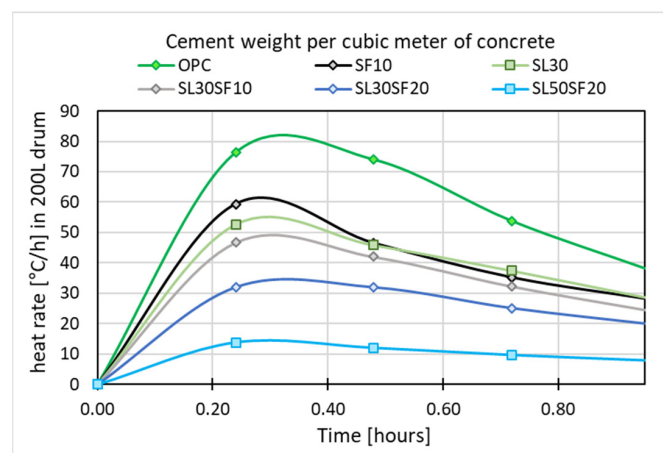
(**b**)

Figure 5. (**a**) Temperature evolution of single, binary, and ternary cemented systems during hydration predicted at the core. (**b**) Heat rate in early hydration of blended systems with different substitution levels.

The hydration heat reduction in SF10 can be explained by the so-called pozzolanic reaction Equation (13). In the first few hours, Ca^{2+} and alkali ions are rapidly produced by the hydration of cement in pore solution. Then, they react with SiO_4^{4-} ions released due to the dissolution of SF. The pozzolanic reaction is an exothermic reaction with a maximum heat of hydration corresponding to 870 J/g of SF [22], which is much higher than 495 J/g for OPC cement. However, the reactivity of SF is lower than most of the clinkers (e.g., C_3S, C_3A) due to a lack of calcium hydroxide; thus, the heat produced from the pozzolanic reaction does not compensate for the heat produced from the hydration of the replaced clinkers, which leads to a slower heat release per unit weight of binder, as seen in Figure 5b.

$$H_4SiO_4 + xCa\,(OH)_2 + (y - x - 2)H_2O \rightarrow xCaOSiO_2yH_2O, \tag{13}$$
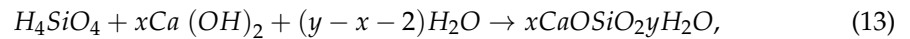
where x is the Ca/Si ratio in C–S–H and y is the molar number of water in C–S–H.

In Figure 5, as for heat reduction due to the addition of BFS in SL30, it is similarly observed compared to SF10, but the effect of the slag reaction is completely different. The slag reaction in an alkaline environment created by the OPC hydration liberates a significant amount of calcium hydroxide. Therefore, slag exhibits both cementitious behavior (latent hydraulic activity) and pozzolanic reactions (with calcium hydroxide) during the formation of the C–A–S–H phase [23]. However, the slag reaction is typically quite slow in low-pH environments because of the low sulfate content. As the sulfate content in BFS is much lower than in OPC, sulfate tends to deplete faster in the presence of BFS (due to adsorption onto C–S–H formed in the hydration of both cement and BFS and C_3A). Therefore, C_3A slowly reacts at a later age to form monosulfoaluminate, as reported in [40].

In addition to the heat reduction due to SCM shown in Figure 5, ternary systems like SL30SF10, SL30SF20, and SL50SF20 show even higher heat reduction during cement hydration than binary cemented systems, and the maximum temperature drops below the DEF threshold temperature thanks to the synergistic effect of SF and BFS on the hydration of cement clinkers. The presence of SF reduces the alkalinity due to the pozzolanic reaction, which as a result lowers the dissolution of BFS, causing a much slower reaction of the BFS [21]. The synergetic effect becomes more evident with the increase in the SF and BFS replacement for the maximum cumulative heat.

In Figure 6, it can be observed that the incorporation of sludge waste increases the hydration heat. For instance, 50% loading of waste sludge (SL30SF10SLu50, SL30SF20SLu50, and SL50SF20SLu50) leads to a temperature rise of approximately 15–20 °C compared to SL30SF10, SL30SF20, and SL50SF20. The increase in heat rate presented in Figure 6b is due to an acceleration of hydration in the cemented waste samples due to the presence of cerium (Ce) in the waste that interacts with aluminate and silicate in the clinkers to form new phases like $CeAl_{11}O_{18}$ and $Ce_{4.667}\,(SiO_4)_3O$ [41]. In addition, the sulfate content of the waste could cause high reactivity in clinkers and SCMs, thus leading to additional heat release. Also, the maximum temperature lowers as SF and BFS replacement ratios increase, which is consistent with the observation of the effect of the replacement ratio on the heat release as described in Section 3.1. This suggests that there is no chemical interaction between SF and BFS with waste sludge.

According to the results above, it is worth mentioning that SCMs can reduce the temperature in ternary systems with/without waste, which could minimize potential DEF. However, DEF is not only influenced by temperature but also by other parameters such as the chemical composition and drum size, which will be discussed in the next sections. The temperature evolution and distribution of different blended systems and drum sizes obtained from the thermal model are incorporated into the chemical model.

(a)

(b)
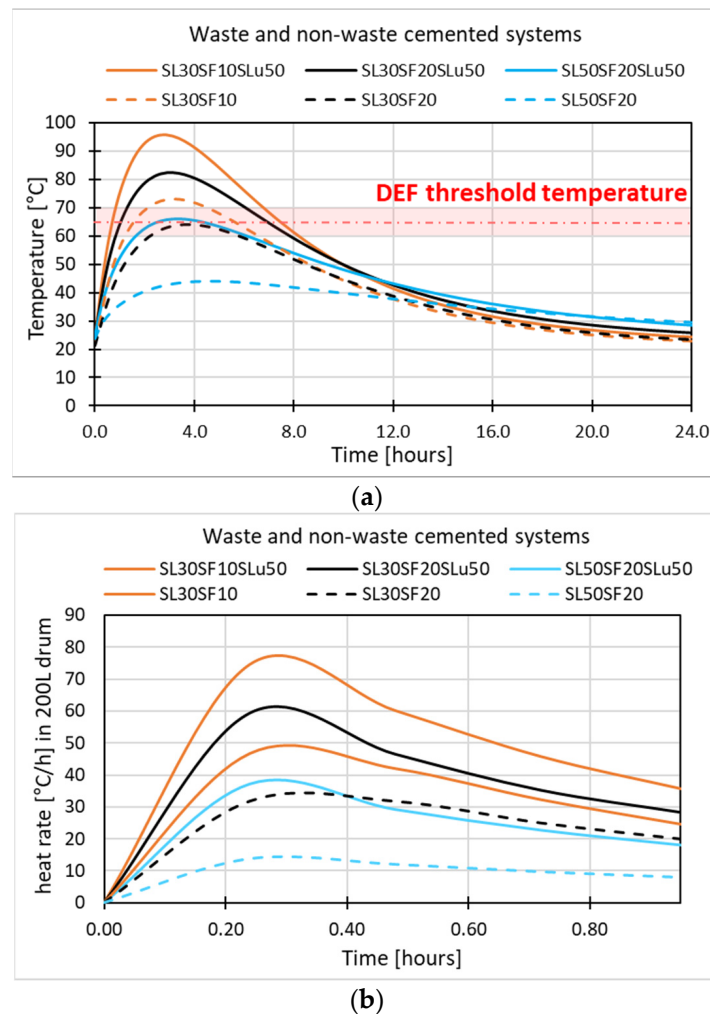
Figure 6. (**a**) Temperature evolution of waste and non-waste cemented samples during hydration predicted at the core. (**b**) Heat rate at early hydration of waste and non-waste cemented samples predicted at the core.

3.2. Influence of Chemical Composition on DEF

Another important parameter that defines DEF formation is the chemical composition of cement. The most significant contributors are the content of SO_3, tricalcium aluminate (C_3A), and alkali content. The equivalent concentrations of sulfate (S_c), aluminate (A_c), and alkali Na_{eq} in the cemented formulations used in this study are shown in Table 5. It should be noted that the equivalent sulfate (here denoted as S_c) is provided by calcium sulfate (gypsum) and the added sulfate from the waste sludge. As for the equivalent moles of aluminate A_c, it represents the concentration of tetracalcium aluminoferrite (C_4AF) and tricalcium aluminate (C_3A) combined.

As mentioned above, the replacement of OPC by SF and/or BFS reduces the hydration heat and changes the overall chemical composition of the mix, and this affects DEF formation. From Table 5, it can be seen that different proportions of BFS, SF, and waste sludge (SL) result in different equivalent sulfate (S_c) and aluminate (A_c) amounts. Moreover, waste sludge that contains 0.12% sulfate trioxide (SO_3) also adds sulfate content to the system since it is mixed in high quantities, as shown in Table 5. According to the chemical formula of ettringite shown in Equation (1), higher amounts of S_c will result in higher amounts of primary hydrates (primary ettringite and monosulfates) and, consequently, in higher amounts of delayed ettringite.

The sulfate–aluminate molar ratio ($\frac{Sc}{Ac}$) is lower than one in all blended systems, and this implies that the DEF is sulfate-dependent, as it happens when there are free sulfate ions in the pore solution. A sensitivity analysis was conducted to investigate the volumetric fraction of delayed ettringite in relation to a variation in the sulfate content. The range of maximum temperature and heating period were chosen as 67–85 °C and 1–8 h, respectively, to represent the period of the hydration heat evolution above the threshold temperature for DEF at the core of the 200 L drum. As for the alkali concentration range, it was constrained to lower values of 0.35–0.60 mol/L to avoid interference with other effects. S_c is defined by the weight of cement per cubic meter and the SO_3 percentage of the material composition. The range of SO_3 and cement weight is 1.0–4.5% and 300–600 kg/m^3, respectively.

In Figure 7b, it is evident that the volumetric fraction of delayed ettringite becomes larger at higher temperatures (65–85 °C) and longer heating periods (but not longer than 8 h), and this increase can be magnified by samples with a high sulfate content (>200 mol/m^3). Figure 7a presents the predicted delayed ettringite fraction at different SO_3 percentages and cement weights per cubic meter of concrete. It shows that in cemented waste samples, the high content of total sulfate S_c (>200 mol/m^3), as seen in Table 5, can result in a large amount of delayed ettringite when the temperature is above the DEF threshold temperature.
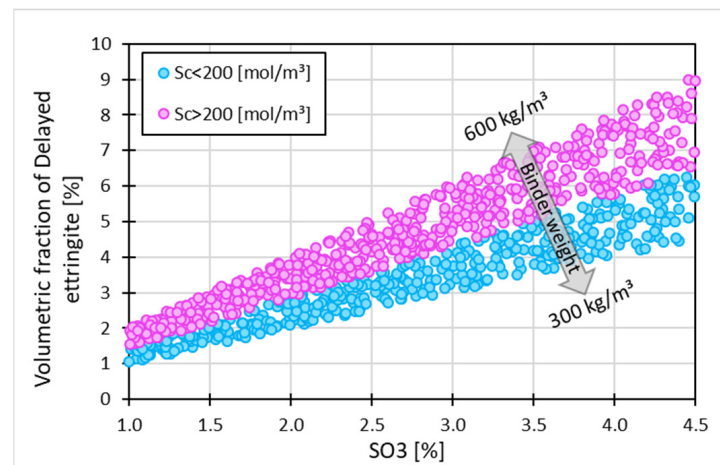
(**a**)
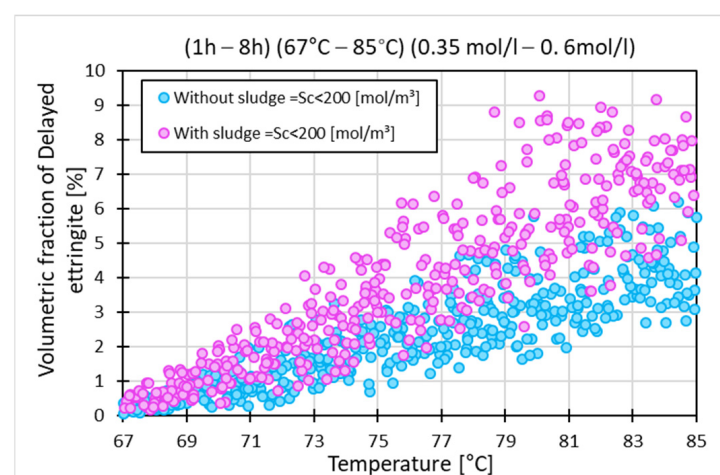
(**b**)

Figure 7. Volumetric fraction of delayed ettringite as a function of (**a**) sulfate trioxide (SO_3%) content per 100 g of cement and cement weight per cubic meter. (**b**) Temperature.

In addition to S_c and A_c, the alkali concentration is also an important parameter for the formation of DEF. Na_{eq} is calculated from the concentrations of Na^+ and K^+ that are computed from the mass fraction and molecular weight. In the chemical model of Sellier and Multon [27], a full dissolution of alkali solid phases is assumed, and alkalis bound in calcium silicate hydrates (C–S–H) matrix are neglected such that all alkali ions (Na^+ and K^+) are available in the pore solution. Since the simulated samples are considered to be contained inside a 200 L drum and are not exposed to the outside environment, alkalis cannot leach out into the surroundings. Hence, the maximum volumetric fraction of delayed ettringite is expected at the core.

$$Na_{eq} = \frac{2\,Na_2O_{eq}}{\varnothing \cdot S_r},$$
(14)

where $\varnothing$ is the porosity, S_r is the degree of water saturation, and Na_2O_{eq} is the equivalent concentration of alkali available in the cement. Figure 8 presents the maximum volumetric fraction of delayed ettringite at different alkali concentrations in the pore solution without leaching. The studied equivalent alkali range represents the concentration that can be found in any cement-based material (cemented waste, blended cement, or controlled OPC samples) used in previous studies [14,15,21,37], and their corresponding DEF is highlighted in Figure 8. Using the mass balance equation of alkali in Equation (14), the conventional alkali content (Na_{eq}) in pore water is computed. It is important to note that the effect of alkali concentration on DEF threshold temperature (ettringite destabilization temperature) is considered in this study using a simplified approach proposed by [27] and derived from Brunetaud's experiments [14]. As Sellier and Multon stated, this approach was chosen instead of employing mass balance equations that consider all relevant chemical species simultaneously [42], which is computationally intensive to use in finite element models.

$$T_{th,d} = \begin{cases} T_{th,ref} & Na < Na_k \\ T_{th,ref}\left(\frac{Na_k}{Na}\right)^n & Na > Na_k \end{cases}'$$
(15)

where $T_{th,ref}$ is the dissolution temperature at a characteristic alkali concentration Na_k of 0.28 mol/L and n is an exponent for the dissolution temperature equal to 0.19. The effect of alkali concentration on the latency time of DEF and the maximum delayed ettringite at different initial alkali concentrations given in Table 5 was evaluated by the sensitivity analysis. In particular, days 300 and 1000 were chosen to investigate the latency period of DEF using the range of maximum temperature, and the heating period was chosen as 67–85 °C and 1–8 h, respectively.

In Figure 8a, it is evident that DEF kinetics are faster at low alkali concentrations. For instance, with an alkali concentration between 0.35 and 0.45 mol/L, delayed ettringite almost reaches its maximum at day 300. On the other hand, higher alkali concentrations in the range of 0.5–0.6 mol/L, which can be found in cemented waste, result in a slower formation of delayed ettringite. At higher alkali concentrations ($Na_{eq} > 0.75$ mol/L), it can be noticed that the volumetric fraction of delayed ettringite is much slower or almost prevented compared to lower alkali values, as shown in Figure 8b, even after 1000 days.

This indicates that different Na_{eq} from different chemical and mortar compositions have a direct impact on the precipitation rate of delayed ettringite, which agrees well with Famy's experiments [16]. In their study, they stated that, at ambient temperature, low alkali concentrations in the pore water can decrease the release rate of sulfate ions from C–S–H, which results in accelerating the precipitation of delayed ettringite. With this observation, it is possible to state that the leaching of alkali from the sample can further shorten the latency time of DEF.

(a)

(b)
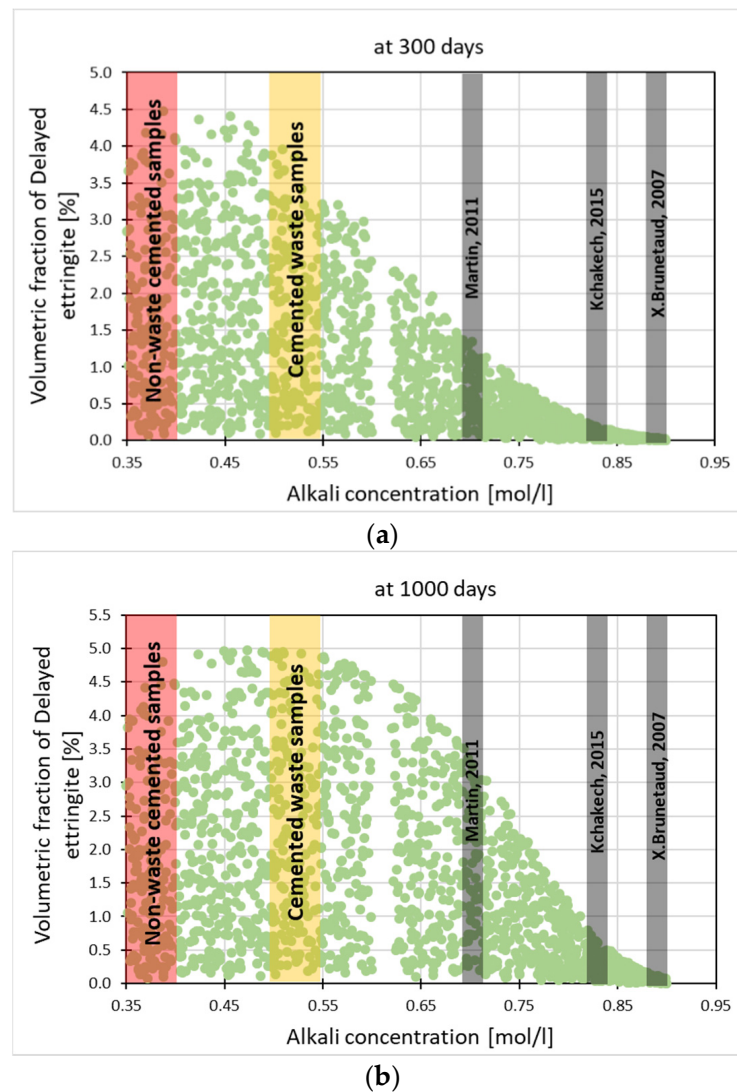
Figure 8. Maximum volumetric fraction of delayed ettringite at different initial alkali concentrations on (**a**) day 300 and (**b**) day 1000 [14,15,36].

3.3. Influence of Drum Size on DEF

As mentioned earlier, the cementation technique for low- and intermediate-level liquid radioactive waste is normally conducted in different drum sizes (commonly 200 L and 400 L in Belgium). Because of the larger volume and dimensions, the temperature distribution and evolution differ and therefore affect the evolution of DEF. The temperature evolution during hydration predicted at the core (0.0, 0.0) of 200 L and 400 L drums, as well as the corresponding maximum volumetric fraction of delayed ettringite, is presented in Figure 9.

It can be seen from Figure 9a that the temperature increases with increasing drum size for similar cemented-waste formulations. In formulations with high replacement ratios, such as SL50SF20SLu50 and SL50SF20SLu45, the DEF threshold temperature is only exceeded in a 400 L drum because of higher heat generation and lower heat dissipation. Compared to smaller drums (200 L), the heat rate becomes higher as the size is enlarged, thus a small volumetric fraction of 2.2% and 1.0% is encountered in SL50SF20SLu50 and SL50SF20SLu45, respectively.

(**a**)

(**b**)
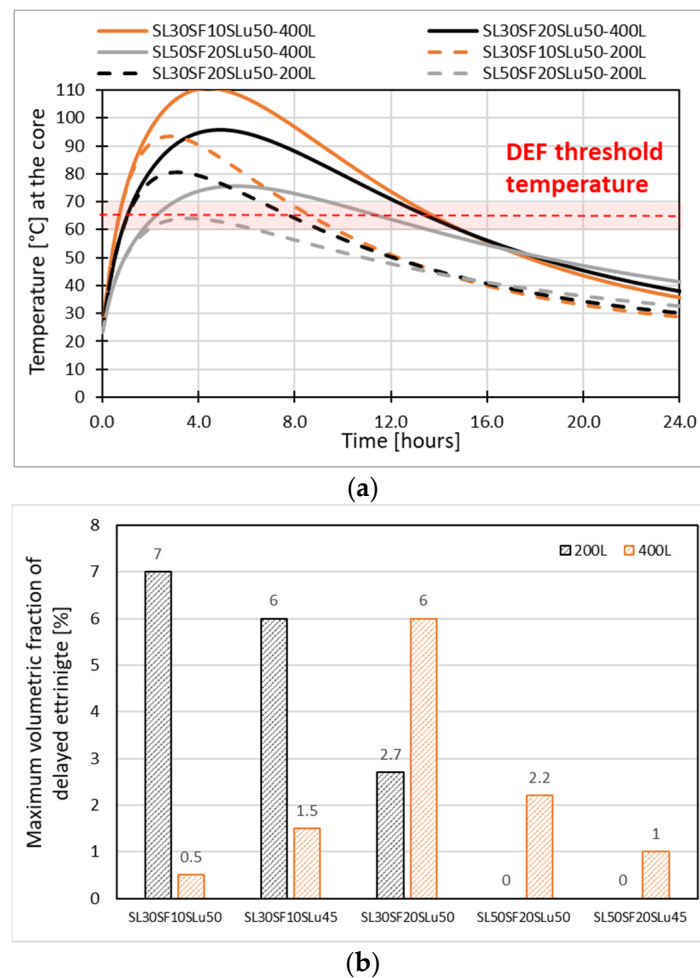
Figure 9. (**a**) Evolution of temperature during hydration predicted at the core of 200 L and 400 L drums. (**b**) Maximum volumetric fraction of delayed ettringite in 200 L and 400 L drums.

On the other hand, in compositions with low SCM replacement ratios such as SL30SF10-SLu50 and SL30SF10SLu45, the effect of drum size on DEF behavior manifests differently despite their high hydration heat. For instance, SL30SF10SLu50_400L and SL30SF10SLu45_400L exhibit much lower DEF than SL30SF10SLu50_200L and SL30SF10SLu45_200L. This behavior can be attributed to the so-called pessimum effect. As demonstrated in [14,15], the pessimum effect occurs when there is a high depletion of free aluminate due to hydrogarnet formation. Because of the low solubility of hydrogarnet, the availability of aluminum for the formation of ettringite is low. Therefore, with the observed pessimum effect in Figure 9b, it is expected to experience different distributions of DEF over the sample as the drum size varies. Besides 200 L and 400 L, several drum sizes are standardized in several countries for typical cemented LILW packaging assigned with a certain drum material and maximum weight [43]. Hence, the pessimum effect on DEF variation across different locations in a range of drum sizes may be encountered. To explore the DEF behavior for different potential drum sizes, sizes ranging from 100 L to 500 L were chosen in this study. The drum height (H) to diameter (D) ratio is assumed to be 1.55, as shown in Figure 10c.

Figure 10a shows the behavior of DEF in SL30SF10SLu50 at different locations in different drum dimensions. It is evident that the maximum amount of delayed ettringite (8.0%) was reached for drum diameters larger than 0.55 m. Moreover, it is interesting to note that the maximum amount of delayed ettringite was encountered in different locations for different drum diameters. For instance, the maximum DEF is encountered at (D/4, H/4) for a drum diameter of 0.78 m (500 L drum) and not at the core (0, 0). According to the evolution of DEF species presented in Figure 10b, the maximum amount of delayed

ettringite is reached when monosulfate is about to be fully depleted. In drums with lower diameters (100 L and 200 L), monosulfate is not fully dissolved, thus the maximum DEF is not encountered, as shown in Figure 10b.
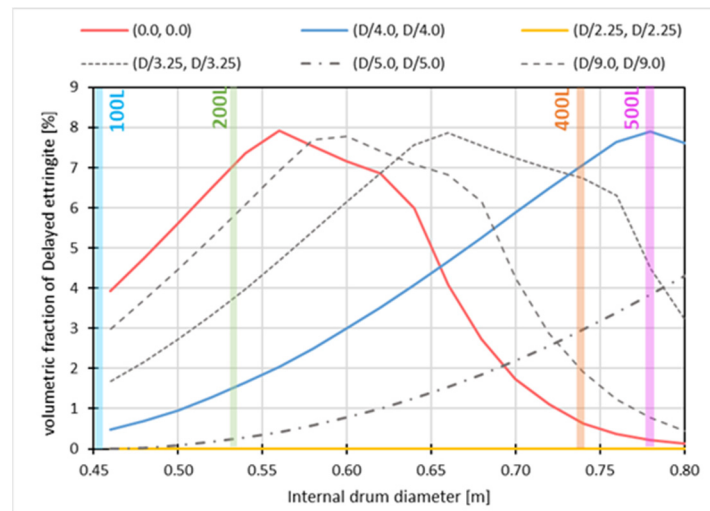
(**a**)
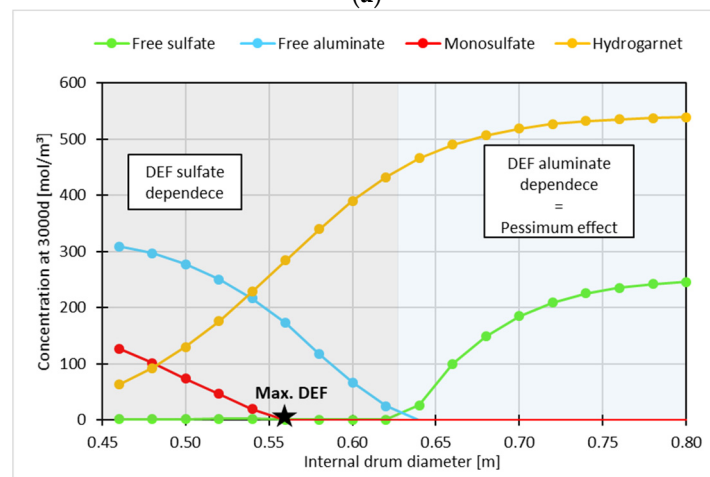
(**b**)
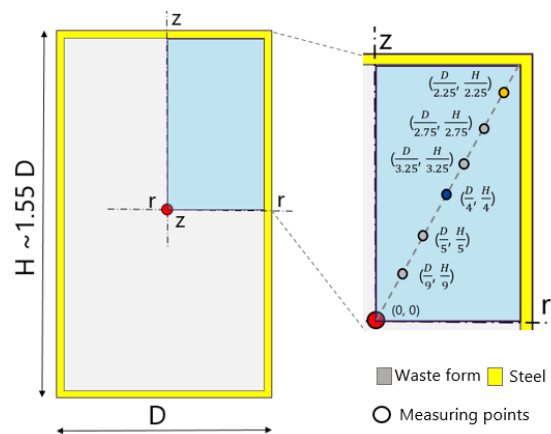
(**c**)

Figure 10. (**a**) Maximum volumetric fraction of delayed ettringite at different locations and different drum diameters. (**b**) Concentration of species associated with DEF estimated at the core (0.0, 0.0) with different drum diameters. (**c**) Drum dimensions and analyzed locations. Black star represents the maximum delayed ettringite can possibly be encountered.

Another observation of the pessimum effect in Figure 10a, in the red curve (DEF estimation at the core), is that larger drum sizes exhibit low DEF despite higher temperatures. This suggests that the pessimum effect becomes more pronounced in larger drums (such as 400 L and 500 L) as the precipitation rate of hydrogarnet increases, which consequently can lead to a much lower free aluminate ion concentration in the pore solution. In this case, the ettringite formation becomes more dependent on the amount of aluminates. This can be observed for the samples SL30SF10SLu50_400L and SL30SF10SLu45_400L, where the temperature goes above 70 °C for a heating period of approximately 12 h, as shown in Figure 9b.

As addressed in Section 3.3, for the effect of chemical composition, sulfate and aluminate represent the main parameters that control the amount of delayed ettringite. With the more pronounced pessimum effect in large drums, it is important to study the amount of delayed ettringite and hydrogarnet with varying aluminate content in blended materials. For this purpose, further chemo–thermal analyses have been carried out wherein the maximum temperature range is set to 85–110 °C with a heating period not longer than 12 h that can be found during hydration at the core of large drums of SL30SF10SLu50_400L and SL30SF20SLu50_400L, as observed in Figure 9a. The results of these analyses are presented in Figure 11a. It can be observed that DEF and hydration temperature are inversely proportional, which further demonstrates the pessimum effect in which the hydrogarnet is formed in high amounts, as seen in Figure 11b. Moreover, this observation is quite opposite to the observed trend in lower maximum temperature (65–85 °C) in Figure 7b.

(**a**)

(**b**)
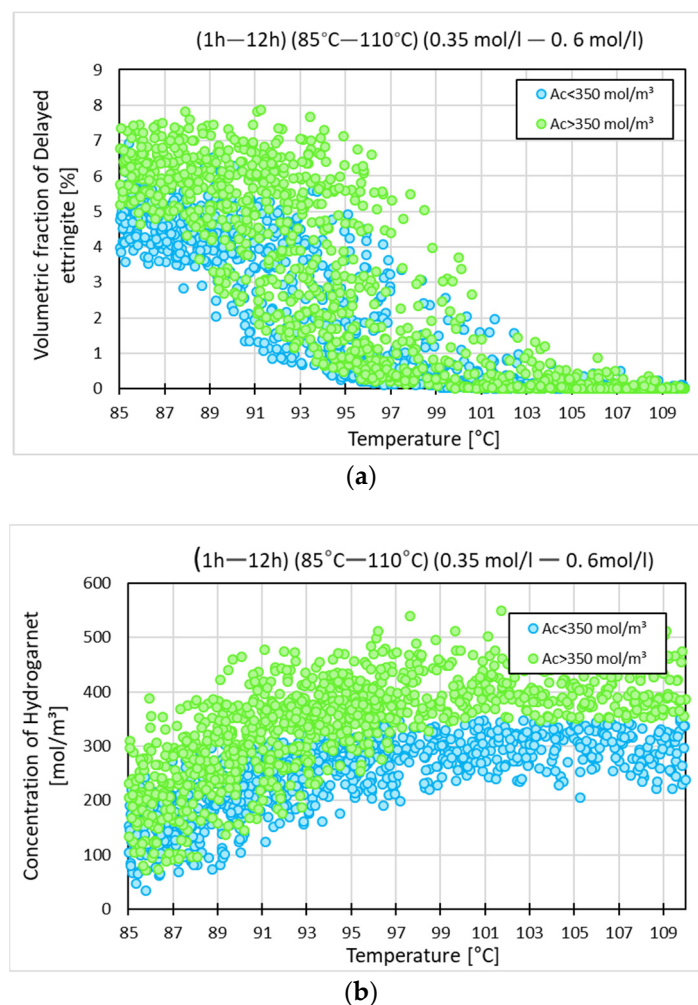
Figure 11. (**a**) Maximum volumetric fraction of delayed ettringite. (**b**) Hydrogarnet concentration at total aluminate content of higher and lower than 350 mol/m^3.

The pessimum effect can be encountered during longer heating periods, even at temperatures lower than 85 °C, as in previous experiments [14,15]. For a longer heating period (4–10 days), the results are presented in Figure 12. The DEF behavior is similar to Figure 11, as there is enough heating period for the total aluminate to convert to hydrogarnet when the temperature is above T_f (70 °C).
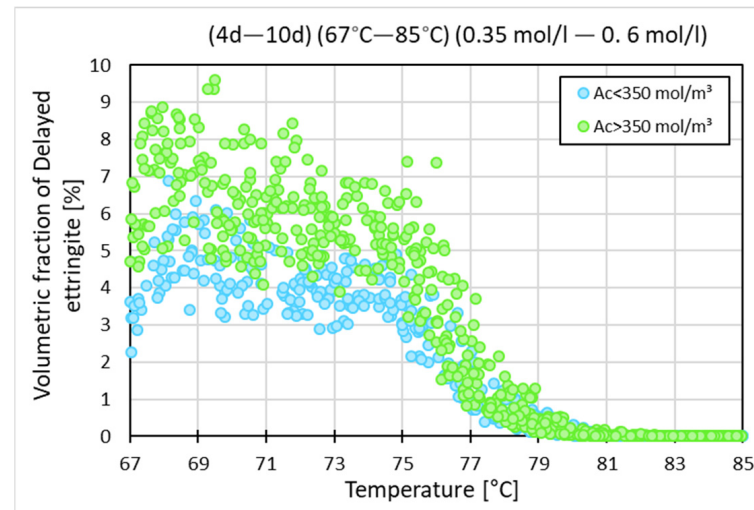
(a)
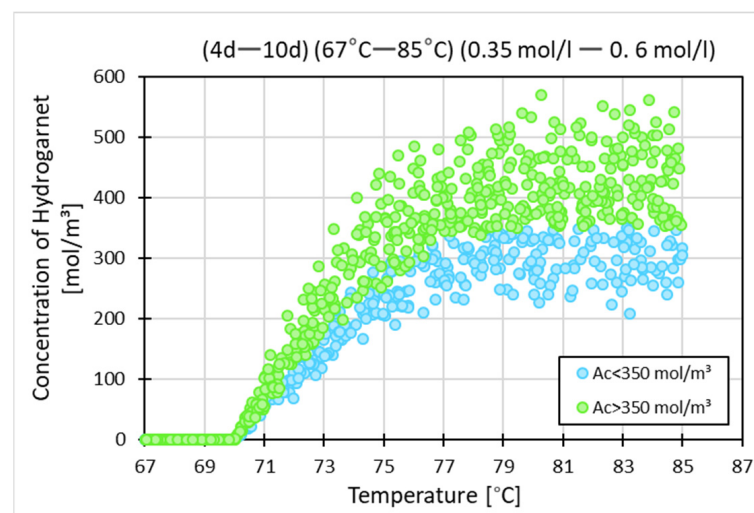
(b)

Figure 12. (**a**) Maximum volumetric fraction of delayed ettringite. (**b**) Hydrogarnet concentration at total aluminate content of higher and lower than 350 mol/m^3.

Using the same sets of inputs, Figure 13 demonstrates the aluminate dependency of delayed ettringite during the pessimum effect. When the maximum temperature is lower than 75 °C, the maximum volumetric fraction of delayed ettringite is linearly promotional to A_c. At higher temperatures, aluminate is fully consumed, resulting in zero or insignificant amounts of delayed ettringite. From Figures 11–13, it is seen that the maximum amount of delayed ettringite increases with initial A_c content during the pessimum effect. At very high temperatures or very long heating periods, the effect becomes more pronounced when a full amount of the aluminate is used for hydrogarnet formation; thus, no delayed ettringite can precipitate.
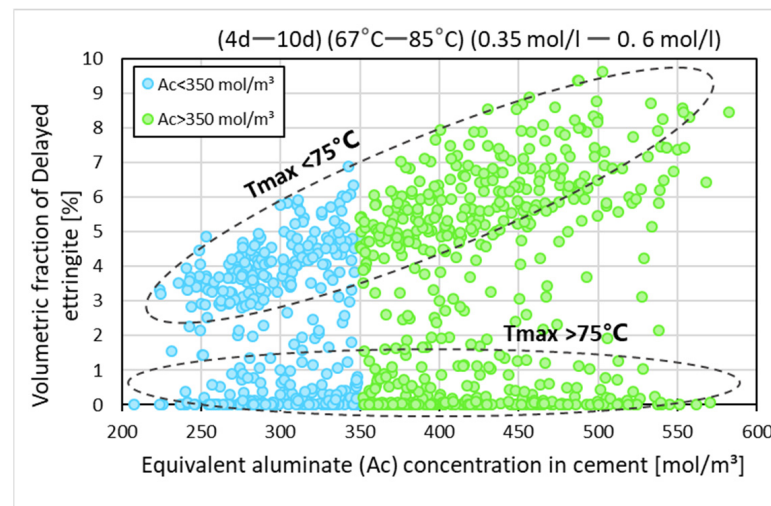
Figure 13. Maximum volumetric fraction of delayed ettringite at different total aluminate contents at different temperatures (65–85 °C).

4. Conclusions and Perspectives

Based on the findings from the chemo–thermal model used to explore the DEF behavior in cemented waste drums with different sizes and replacement ratios of SCM, the following conclusions can be drawn:

- Partial replacements of OPC by SCMs have been proven to be a suitable measure in reducing the heat hydration heat in small drum sizes (200 L or lower), which results in a lower potential for DEF;
- The contribution of the additional heat generated by the waste–cement interaction to the DEF is higher with lower SCM replacement ratios;
- Maximum delayed ettringite is proportional to the sulfate content when the temperature exceeds the DEF threshold temperature for a heating period of up to 8 h. Additional sulfate content from sludge waste (sulfuric) results in higher amounts of delayed ettringite for smaller drums (200 L or lower);
- In larger drums with low SF and BFS additions, the maximum amount of delayed ettringite at the core switches from sulfate dependence to aluminate dependence due to the pessimum effect;
- In cases with significantly high temperatures or long heating periods, the pessimum effect becomes more pronounced, and DEF is not encountered;
- The precipitation of delayed ettringite in waste-containing blended systems is slower due to higher initial alkali concentrations in the pore solution compared to blended systems without waste;
- It seems preferable to use ternary systems (OPC–SF–BFS) and drum sizes not larger than 200 L to minimize DEF potential in cemented waste forms.

The proposed coupled thermo–chemical model can be adopted to design a DEF experimental plan for DEF characterization purposes. However, a high-order sensitivity analysis (accounting for synergetic effects) is needed to study the correlation of the input parameters with DEF, which will be the subject of a future study. Furthermore, our forthcoming research involves performing specific experiments and thermodynamic studies that focus on phase assemblages and allow for quantification of Al-based phases (such as C–A–S–H, hydrotalcite, strätlingite, and third aluminate hydrates) formed in binary (OPC–BFS) or ternary (OPC–BFS–SF) cemented systems. This will enable us to consider the suppression effect on DEF expansion and validate the predicted DEF in different blended systems. This topic represents a subject that will be addressed in a future study conducted within the framework of the first author's research.

References

1.　IAEA. *Nuclear Power and Sustainable Development*; IAEA: Vienna, Austria, 2016.
2.　Pearce, J.M. Limitations of Nuclear Power as a Sustainable Energy Source. *Sustainability* **2012**, *4*, 1173–1187. [CrossRef]
3.　IAEA. *IAEA Safety Glossary, Terminology Used in Nuclear Safety and Radiation Protection*; IAEA: Vienna, Austria, 2019.
4.　Ojovan, M.I.; Lee, W.E. Immobilisation of Radioactive Wastes in Cement. In *An Introduction to Nuclear Waste Immobilisation*; Elsevier: Amsterdam, The Netherlands, 2014; pp. 205–232. [CrossRef]
5.　Łowińska-Kluge, A.; Piszora, P. Effect of Gamma Irradiation on Cement Composites Observed with XRD and SEM Methods in the Range of Radiation Dose 0-1409 MGy. *Acta Phys. Pol. A* **2008**, *114*, 399–411. [CrossRef]
6.　Heath, T.; Schofield, J.; Shelton, A. Understanding Cementitious Backfill Interactions with Groundwater Components. *Appl. Geochem.* **2020**, *113*, 104495. [CrossRef]
7.　Stefan, L.; Varet, T.; Lamouroux, C. In Proceedings of the 44th Annual Waste Management Conference (WM2018) Nuclear and Industrial Robotics, Remote Systems and Other Emerging Technology, Phoenix, AZ, USA, 18–22 March 2018; Waste Management Symposia Inc.: Tempe, AZ, USA, 2018; Volume 1.
8.　Taylor, H.F.W.; Famy, C.; Scrivener, K.L. Delayed Ettringite Formation. *Cem. Concr. Res.* **2001**, *31*, 683–693. [CrossRef]
9.　Thomas, M.; Folliard, K.; Drimalas, T.; Ramlochan, T. Diagnosing Delayed Ettringite Formation in Concrete Structures. *Cem. Concr. Res.* **2008**, *38*, 841–847. [CrossRef]
10.　Phung, Q.T.; Maes, N.; Jacques, D. *Current Concerns on Durability of Concrete Used in Nuclear Power Plants and Radioactive Waste Repositories*; Lecture Notes in Civil Engineering (LNCE); Ho Chi Minh City University of Technology: Thành phố Hồ Chí Minh, Vietnam, 2017; ISBN 9789811067129.
11.　Amde, A.M.; Ceary, M.; Livingston, R.A.; McMorris, N. *Pilot Field Survey of Maryland Bridges for Delayed Ettringite Formation Damage*; The University of Maryland: Baltimore, MD, USA, 2004.
12.　Godart, B.; Divet, L. Lessons Learned from Structures Damaged by Delayed Ettringite Formation and the French Prevention Strategy. In Proceedings of the Fifth International Conference on Forensic Engineering, Institution of Civil Engineers, London, UK, 16–17 April 2013.
13.　Wimpenny, D.E.; White, P.S.; Eden, M.A. Two Case Studies of the Management of Bridges Diagnosed with Delayed Ettringite Formation. In *Bridge Design, Construction and Maintenance*; Institution of Civil Engineers: London, UK, 2007; pp. 448–457. [CrossRef]
14.　Brunetaud, X.; Linder, R.; Divet, L.; Duragrin, D.; Damidot, D. Effect of Curing Conditions and Concrete Mix Design on the Expansion Generated by Delayed Ettringite Formation. *Mater. Struct. Constr.* **2007**, *40*, 567–578. [CrossRef]
15.　Kchakech, B. Badreddine KCHAKECH Etude de l'Influence de l'Échauffement l'Échauffement Subi Par Un Béton Sur Le Risque d'Expansions Associées à La Réaction Sulfatique Interne. Ph.D. Thesis, Université Paris-Est, Paris, France, 2015.
16.　Famy, C.; Scrivener, K.L.; Atkinson, A.; Brough, A.R. Influence of the Storage Conditions on the Dimensional Changes of Heat-Cured Mortars. *Cem. Concr. Res.* **2001**, *31*, 795–803. [CrossRef]
17.　Gu, Y. Experimental Pore Scale Analysis and Mechanical Modeling of Cement-Based Materials Submitted to Delayed Ettringite Formation and External Sulfate Attacks. Ph.D. Thesis, Université Paris-Est, Paris, France, 2018.
18.　Nanayakkara, A. Importance of Controlling Temperature Rise Due To Heat of Hydration in Massive Concrete Elements. *Soc. Soc. Manag. Syst. Internet J.* **2011**, 502–508. Available online: http://dl.lib.mrt.ac.lk/handle/123/12394 (accessed on 29 October 2023).
19.　Pichelin, A.; Carcassès, M.; Cassagnabère, F.; Multon, S.; Nahas, G. Sustainability, Transfer and Containment Properties of Concrete Subject to Delayed Ettringite Formation (DEF). *Cem. Concr. Compos.* **2020**, *113*, 103738. [CrossRef]
20.　Moon, H.; Ramanathan, S.; Suraneni, P.; Shon, C.S.; Lee, C.J.; Chung, C.W. Revisiting the Effect of Slag in Reducing Heat of Hydration in Concrete in Comparison to Other Supplementary Cementitious Materials. *Materials* **2018**, *11*, 1847. [CrossRef]

21. Phung, Q.T.; Ferreira, E.; Seetharam, S.; Nguyen, V.T.; Govaerts, J.; Valcke, E. Understanding Hydration Heat of Mortars Containing Supplementary Cementitious Materials with Potential to Immobilize Heavy Metal Containing Waste. *Cem. Concr. Compos.* **2021**, *115*, 103859. [CrossRef]

22. Kadri, E.H.; Duval, R. Hydration Heat Kinetics of Concrete with Silica Fume. *Constr. Build. Mater.* **2009**, *23*, 3388–3392. [CrossRef]

23. Kolani, B.; Buffo-lacarrière, L.; Sellier, A.; Escadeillas, G.; Boutillon, L.; Linger, L. Hydration of Slag-Blended Cements. *Cem. Concr. Compos.* **2012**, *34*, 1009–1018. [CrossRef]

24. Chen, J.; Qian, C.; Song, H. A New Chemo-Mechanical Model of Damage in Concrete under Sulfate Attack. *Constr. Build. Mater.* **2016**, *115*, 536–543. [CrossRef]

25. Chanvilard, G.; Barbarulo, R. Stress From Confined Crystallization Occurring by Internal Phase Change: Application to the Case of Delayed Ettringite Formation in Hardened Cement Paste. In *Mechanics and Physics of Porous Solids*; Wiley: Hoboken, NJ, USA, 2011; pp. 1–23.

26. Flatt, R.J.; Scherer, G.W. Thermodynamics of Crystallization Stresses in DEF. *Cem. Concr. Res.* **2008**, *38*, 325–336. [CrossRef]

27. Sellier, A.; Multon, S. Chemical Modelling of Delayed Ettringite Formation for Assessment of Affected Concrete Structures. *Cem. Concr. Res. J.* **2018**, *108*, 72–86. [CrossRef]

28. Ramlochan, T.; Zacarias, P.; Thomas, M.D.A.; Hooton, R.D. The Effect of Pozzolans and Slag on the Expansion of Mortars Cured at Elevated Temperature: Part I: Expansive Behaviour. *Cem. Concr. Res.* **2003**, *33*, 807–814. [CrossRef]

29. Ramlochan, T.; Thomas, M.D.A.; Hooton, R.D. The Effect of Pozzolans and Slag on the Expansion of Mortars Cured at Elevated Temperature: Part II: Microstructural and Microchemical Investigations. *Cem. Concr. Res.* **2004**, *34*, 1341–1356. [CrossRef]

30. Kawabata, Y.; Takahashi, H.; Watanabe, S. The Long-Term Suppression Effects of Fly Ash and Slag on the Expansion of Heat-Cured Mortar Due to Delayed Ettringite Formation. *Constr. Build. Mater.* **2021**, *310*, 125235. [CrossRef]

31. Nguyen, V.H.; Leklou, N.; Aubert, J.E.; Mounanga, P. The Effect of Natural Pozzolan on Delayed Ettringite Formation of the Heat-Cured Mortars. *Constr. Build. Mater.* **2013**, *48*, 479–484. [CrossRef]

32. Rida, L.; Alaoui, A.H. Effect of High Volume Fly Ash and Curing Temperature on Delayed Ettringite Formation. *Mater. Today Proc.* **2022**, *58*, 1285–1293. [CrossRef]

33. Mckay, M.D.; Beckman, R.J.; Conover, W.J. A Comparison of Three Methods for Selecting Values of Input Variables in the Analysis of Output From a Computer Code. *Am. Stat. Assoc. Am. Soc. Qual.* **1979**, *42*, 55–61.

34. Hora, S.C.; Helton, J.C. A Distribution-Free Test for the Relationship between Model Input and Output When Using Latin Hypercube Sampling. *Reliab. Eng. Syst. Saf.* **2003**, *79*, 333–339. [CrossRef]

35. Kothari, C.; Takahashi, Y. The Effect of Heat Treatment on the Kinetics of the Delayed Ettringite Formation—An Improved Chemo-Thermal-Hygral Model. *Constr. Build. Mater.* **2022**, *331*. [CrossRef]

36. Renaud-Pierre, M. Analyse sur Structures Modèles des Effets Mécaniques de la Réaction Sulfatique Interne du Béton. Ph.D. Thesis, Université Paris-Est, Paris, France, 2011.

37. Al Shamaa, M.; Lavaud, S.; Divet, L.; Nahas, G.; Torrenti, J.M. Coupling between Mechanical and Transfer Properties and Expansion Due to DEF in a Concrete of a Nuclear Power Plant. *Nucl. Eng. Des.* **2014**, *266*, 70–77. [CrossRef]

38. Poole, J.L.; Riding, K.A.; Folliard, K.J.; Juenger, M.C.G.; Schindler, A.K. Methods for Calculating Activation Energy for Portland Cement. *ACI Mater. J.* **2007**, *104*, 86–94. [CrossRef]

39. Langan, B.W.; Weng, K.; Ward, M.A. Effect of Silica Fume and Fly Ash on Heat of Hydration of Portland Cement. *Cem. Concr. Res.* **2002**, *32*, 1045–1051. [CrossRef]

40. Meinhard, K.; Lackner, R. Multi-Phase Hydration Model for Prediction of Hydration-Heat Release of Blended Cements. *Cem. Concr. Res.* **2008**, *38*, 794–802. [CrossRef]

41. Motny, R.M.; Phongikaroon, S. Effects of Cerium Concentration and Solvent on Physical and Chemical Characterization of Rapid Setting Cement. *Nucl. Technol.* **2019**, *205*, 671–683. [CrossRef]

42. Damidot, D.; Glasser, F.P. Thermodynamic Investigation of the $CaO-Al_2O_3-CaSO_4-H_2O$ system at 50 °C and 85 °C. *Cem. Concr. Res.* **1992**, *22*, 1179–1191. [CrossRef]

43. IAEA. *Interim Storage of Radioactive Waste Packages*; IAEA: Vienna, Austria, 1998; p. 100.